coatings

MDPI

Article

Reducing Static and Impact Ice Adhesion with a Self-Lubricating Icephobic Coating (SLIC)

Edem Tetteh * and Eric Loth

Department of Mechanical and Aerospace Engineering, University of Virginia, Charlottesville, VA 22904, USA; loth@virginia.edu

* Correspondence: fet8ma@virginia.edu

Received: 10 February 2020; Accepted: 5 March 2020; Published: 11 March 2020

Abstract: Ice accumulation and adhesion can problematically occur on many engineering systems, such as electrical power networks, wind turbines, communication towers, and aircraft. An optional solution to these icing problems is the use of surfaces/coatings with low ice adhesion properties: Icephobic surfaces. Icephobic surfaces/coatings are very beneficial, as they facilitate the removal of ice or retard its formation and do not require the use of any sort of energy. A compact icing research tunnel (CIRT) was employed to measure ice tensile adhesion strength for both impact and static ice on a conventional metal surface (aluminum) and on a Self-Lubricating Icephobic Coating (SLIC) surface. The static ice consisted of deionized water slowly poured over the surface and left to be frozen on the test specimen surface at stationary conditions, while impact ice consisted of droplets of mean volumetric diameter (MVD) of 13 μm impacting the test specimen surface at a velocity of 40 m/s and freezing and accreting dynamically. The results revealed that static ice has an ice tensile adhesion stress higher than that of impact ice for the conditions used, consistent with previous studies. Additionally, a reduction of more than half was observed in ice tensile adhesion stress for SLIC compared to aluminum for both impact and static ice, and this performance stayed consistent even after multiple icing tests on the same sample. The SLIC coating hydrophobicity (roll-off angle and contact angle) also demonstrated resilience to icing and mechanical abrasion, confirming the self-healing properties.

Keywords: ice tensile adhesion; icephobic; aerospace impact ice; static ice; mechanical durability; self-healing

1. Introduction

Atmospheric ice accretion is a great concern for several engineering applications. Ice buildup on aircraft (wings, engine) was recognized to be a serious hazard to flight safety and aircraft operations [1]. Particularly for engines, ice accretion on various components (as shown in Figure 1a) was reported to result in problems such as engine rollback, compressor stall/surge, and flameout. Tragic cases of flight crashes due to icing include the Continental Connection Flight 3407 killing all its passengers [2], the American Eagle Flight 4184 [3], and many others. Other applications that suffer heavily from icing are wind turbines. Ice accumulation on wind turbine blades, as shown in Figure 1b, modifies their aerodynamic characteristics, resulting in a decrease of power production [2,4,5]. Up to a 17% loss in Annual Energy Production (AEP) and a power coefficient reduction into the range of 20–50% were reported for wind turbines due to icing [4]. Furthermore, ice accretion on these blades and irregular shedding typically result in load imbalances and, subsequently, in an excessive turbine vibration [6].

To then prevent or mitigate icing, anti-icing/deicing systems are used. These systems range from active systems, such as electro-thermal systems, to passive systems, such as water-repellent/low adhesion coatings or surfaces. Among these anti-icing/deicing systems, passive systems are more

attractive, as they do not require the use of any sort of energy. One example of passive anti-icing/deicing systems is superhydrophobic coating. These coatings, which have a high degree of water repellency, displayed a low adhesion property, thus proficient at removing/mitigating ice [7–19]. In addition to being icephobic, one of the main issues hindering the large-scale use of superhydrophobic surfaces is their poor mechanical stability. These superhydrophobic surfaces were revealed to be fragile to mechanical shear and usually deteriorated after several trials of the same experiment [18,20–24]. Subsequently, they fail to mitigate ice for long durations in practical conditions. To address this issue of durability of superhydrophobic coatings, techniques such as the introduction of hierarchical roughness structures to reduce the surface roughness features were used to enhance their robustness to mechanical shear [20–24]. In some cases, these techniques helped these surfaces gain self-healing capabilities [21,25]. However, some of these coatings may have additional issues in addition to their mechanical stability. Some studies reported some of these surfaces to perform poorly in environments that were highly humid [18,26,27], at extremely cold temperatures (−15 °C and below) [28], and at conditions besides static ice conditions (i.e., motionless water frozen on a cold surface) or low droplet impact velocities, e.g., less than 10 m/s [29,30]. Additional drawbacks undermining the icephobic properties of these surfaces are described in References [11,28,31–34]. As a result, the association of icephobicity with superhydrophobic surfaces remains debatable.

Another example of passive anti-icing/deicing systems is that of lubricated micro-/nano-textured surfaces infused with hydrophobic or hydrophilic lubricants. These surfaces are widely known as slippery liquid-infused porous surfaces (SLIPS) or liquid-impregnated/infused surfaces (LIS) [27,32,35–42]. These surfaces, which generally possess a low contact angle hysteresis (difference between advancing and receding contact angles) and, in some cases, can self-heal (by capillary wicking due to the lubricating film) [36,37,40,41,43], were highly successful at delaying ice nucleation and achieving low ice adhesion, arguably much better than superhydrophobic surfaces. However, these surfaces' effectiveness may be limited by their mechanical and lubricant stability, as they often lose icephobicity once the lubricating film is depleted (either by evaporation, leak, or consumption) [38,42]. As a result, this may hinder their practical applications [3,39].

A third example of passive anti-icing/deicing systems, which are a sub-branch of SLIPS, is that of liquid-infused elastomers [42,44–49]. Since elastomers generally have a high elastic modulus and elasticity was identified as key to icephobicity [50,51], these surfaces, therefore, combine the use of a lubricant and an elastomer. These liquid-infused elastomers, which consist of an elastic matrix/elastomer in which the lubricant is infused, were revealed to be durable (having self-healing capability) and to possess formidable icephobic properties. One of those surfaces, which showed significant success under supercooled droplets at low impact speeds (less than 10 m/s) is the Self-Lubricating Icephobic Coating (SLIC). SLIC was developed and tested for aerospace applications and showed self-healing properties for these conditions [3]. This coating was found to be stable in long-term centrifugal accelerations in a rotating fan assembly. In particular, the coating applied on a fan blade at a radius of up to 25 cm was rotated at 1000 rpm for up to six hours with no delamination or loss of ice adhesion performance. It should be noted that this corresponds to a centrifugal acceleration of 2,740 m/s^2 (equivalent to 280 g's).

The goal of this study was to investigate the performance of SLIC in terms of tensile ice adhesion for both static ice and high-impact ice (at 40 m/s), and also to directly compare these results to ice adhesion on a surface of aluminum, which represents the most common conventional aerospace metal surface. A specialized Compact Icing Research Tunnel (CIRT) was developed for this study, where the impact ice condition employs a spray cloud of supercooled water droplets, with a mean volumetric diameter (MVD) of 13 μm impacting at a velocity of about 40 m/s in a wind tunnel test section. The CIRT was equipped with a wide array of diagnostics to help fully characterize testing conditions and to obtain ice adhesion tensile strength for both surfaces with a well-established pressure-removal technique. The tensile stress results were then compared to each other and to other tensile stress data available in the literature.

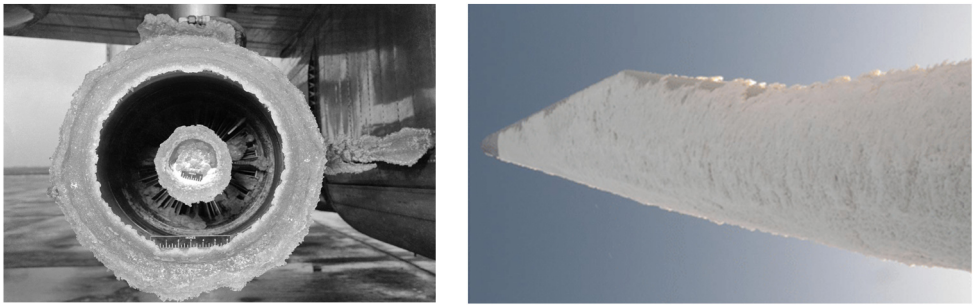

(**a**) (**b**)

Figure 1. Icing on (**a**) the inlet of an aircraft's engine (courtesy of NASA) [52,53] and (**b**) a wind turbine blade [4].

This is a unique study, as ice adhesion has not been previously investigated (to the authors' knowledge) for a self-healing icephobic surface at high-speed (30 m/s and up) impact ice conditions with direct comparison to an aluminum surface. This study is also unique in that it is the first to include a direct comparison of impact ice adhesion data to static ice adhesion data within the same facility. Additionally, this study is the first to compare the robustness of the coating hydrophobicity (contact angle and roll-off angle) for impact icing with that for mechanical abrasion. This abrasion included both a soft abradant (that can cause surface lubricant depletion) and hard abradant (that can cause elastomer depletion).

2. Materials and Methods

2.1. Tested Surfaces

For this study, the surface discs to be tested included a conventional aluminum surface (non-coated) and an aluminum surface coated with SLIC. The SLIC coating is a hydrophobic oil-infused elastomer that was drop-casted on the aluminum substrate. The coating consists of an elastic matrix in which a lubricant (oil in this study) is infused. Different images of the SLIC are shown in Figure 2. As depicted in Figure 2a, the elastomer/elastic matrix acts as a reservoir for the lubricant, which diffuses towards the coating surface. Reference [44] described such a phenomenon where organic lubricants stored within an elastomeric matrix were observed to migrate towards the surface. This lubricant migration towards the surface creates an oil layer at the surface of the coating (shown in Figure 2a–c), which enables it with a low contact angle hysteresis and smoothness (smooth and lubricated part of SLIC is shown in Figure 2d by the dark/gray regions). These characteristics, in addition to the elasticity of the elastomer, are desirable attributes of an effective icephobic surface. Additionally, the constant oil secretion within the coating and diffusion to the surface enables it with a self-healing ability, which will be assessed and described in a section below. The wettability properties of the coating were quantified, as well as the ones of the aluminum, using a Rame-Hart goniometer (Rame-hart Instrument Co., Succasunna, NJ, USA). The contact angles were measured using a 10 µL water drop, while the roll-off angles were measured with a 20 µL water drop. Three measurements were taken on each sample using 3 different drops respectively for the contact and roll-off angles. The average values from the results ensuing from the measurements are tabulated in Table 1. Additionally, the uncoated aluminum substrate (used for comparison) had a roughness R_a of 4.8 µm, while the SLIC coating had a roughness R_a of 1.2 µm and was about 125 µm thick.

Table 1. Wettability properties (contact and roll-off angles) of both aluminum and SLIC surfaces.

Wettability Properties	Aluminum	SLIC
Contact Angle (°)	82.4	99
Roll-off Angle (°)	27	13

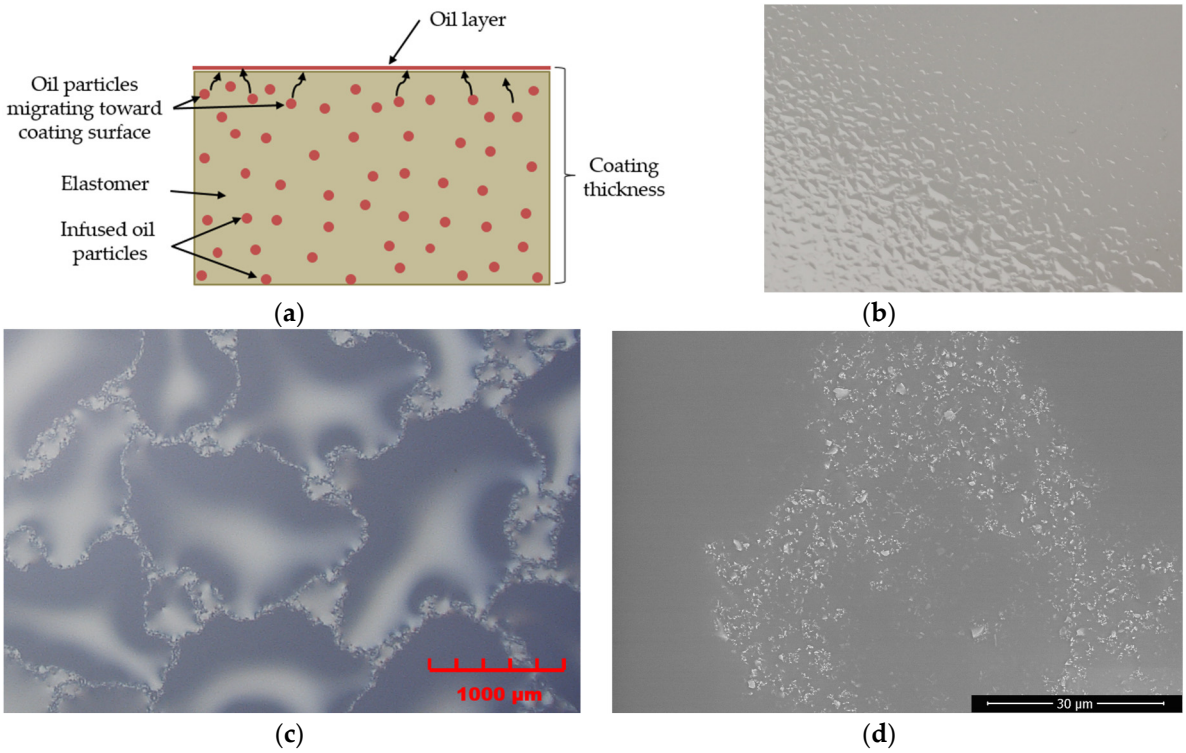

Figure 2. Different images of the Self-Lubricating Icephobic Coating (SLIC) coating: (**a**) Schematic of the SLIC showing the diffusion of the infused oil particles [3], (**b**) a CANON photographic camera picture of SLIC showing the layer of oil atop the elastomer, (**c**) a HIROX optical microscope image of SLIC, where bubbles represent oil atop the elastomer, and (**d**) a scanning electron microscope image showing smooth and lubricated regions of SLIC. These smooth regions are without grains.

2.2. Ice Tensile Facility

The tensile ice adhesion experiments were performed in a compact icing research tunnel (CIRT) located at the University of Virginia, USA. The CIRT has a test section of 7.5 (3″) by 10 cm (4″) and allows icing tests for both static and impact (up to 40 m/s air velocity) conditions [54]. The CIRT was equipped with diagnostics to characterize test conditions and obtain ice tensile adhesion strength on the test specimens. The overall experimental setup is shown in Figure 3a, where the test specimen consisted of a vertical aluminum boss piece (cylinder) coupled to a 30 mm diameter substrate disc.

As shown in Figure 3b, the static ice was obtained by pouring deionized water into a cylindrical mold formed above the test specimen and allowed to freeze over time at an ambient air temperature of –20 °C. The impact ice, on the other hand, was created by spraying an icing droplet cloud with a size of 13 µm and a liquid water content (LWC) of 2.8 g/m^3 0.9 m upstream of the test specimen, as shown in Figure 3a,c. These droplets then impacted the test specimen in the test section at a velocity of 40 m/s, freezing in the process. For both impact and static ice, deionized water was used, as impurities in the water can potentially result in a larger variation in ice adhesion strength [31,55].

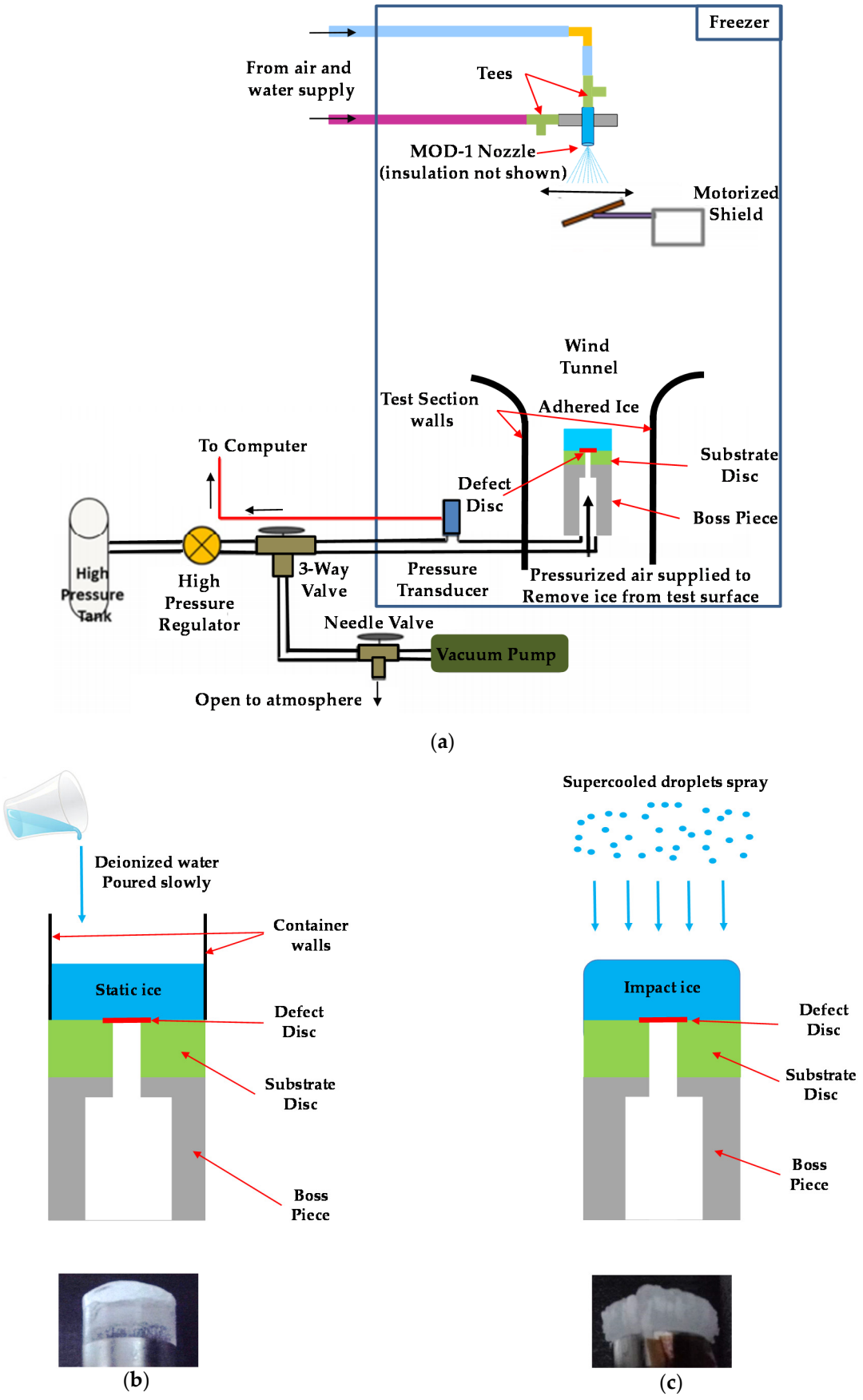

Figure 3. For ice tensile measurements (not to scale): (**a**) Overall setup in the compact icing wind tunnel, (**b**) zoom-in of the static ice accretion procedure, and (**c**) zoom-in of the impact ice accretion procedure.

At the center of the test fixture was a 4 mm diameter hole, which was covered by a thin (50 μm thick) Teflon (PTFE) disc, which was 7 mm in diameter. The purpose of this Teflon disc was to create a sealed surface during both impact and static ice accretion. No recess was needed in the substrate disc for the Teflon disc, as the Teflon disc was maintained firmly on the disc by creating a suction force that was carefully calibrated and controlled by a needle valve attached to a vacuum pump, as shown in Figure 3a. Once ice (impact or static) was established on the substrate disc, pressure from a gas (clean and filtered air from a pressurized air bottle) was applied underneath the Teflon defect via the 4 mm channel to remove most or all of the ice from the substrate in tensile mode. This pressure was initialized at atmospheric conditions and then slowly and continuously increased at a constant rate of 131 kPa/s until ice fracture occurred from the test substrate, a pressure that was labeled as the fracture pressure. This method of ice adhesion measurement on a surface was initially designed and implemented by Andrews and Lockington [56–58], and was adapted to enable in situ testing in an icing wind tunnel for both impact and static ice conditions. More details on this procedure are discussed in the following section.

2.3. Ice Tensile Test Procedures

Prior to each aluminum surface icing test, the substrate disc was cleaned by wiping its surface first with a dry Chem-wipe and then with a Chem-wipe soaked in 95% isopropyl alcohol. A single physical aluminum test substrate was used for all impact and static ice tests. This was to reduce variation in test results that could be attributed to differences in substrate disc characteristics. Similarly, one SLIC test substrate was respectively used for all impact ice tests and one for all static ice tests in order to investigate surface resilience to icing conditions. To prevent any contamination (dirt, dust) on the SLIC surface between icing tests or after, the test substrates were preserved in an enclosed box and were only taken out for icing tests.

Once the aluminum and SLIC test substrate surfaces were ready, they were attached to the boss piece, and the assembly (boss piece and substrate disc) was mounted onto the air pressure pipe in the icing tunnel test section (as shown in Figure 3a). In the case of the static ice tests, a small amount of high-viscosity grease was utilized in addition to the suction force to secure the Teflon disc over the 4 mm access hole of the substrate disc. The high-viscosity grease was added to prevent water from leaking underneath the Teflon disc into the pressurization channel and then freezing over time. This grease was carefully applied to ensure that there was no contamination to the rest of the substrate disc surface. After mounting the test sample in the tunnel test section, the icing wind tunnel ambient air was then set to reach a temperature of −25 °C. The reason for setting the target temperature lower than the intended testing temperature (−20 °C) was to prevent the cooling system of the icing wind tunnel from switching off once the targeted temperature was reached. For both impact and static ice tests, the test substrate was left to cool down to the temperature of −20 °C before ice fracture initiation to reduce variation in test results. The ice fracture procedure for both impact and static ice tensile tests was consistent with that previously established [54]. GoPro recordings of the impact ice accretion, as well as of the tensile test/pop-off test on both the aluminum and SLIC surfaces, are provided in the Supplementary Materials.

A time sequence of all of the steps for the impact ice tensile test is depicted in Figure 4a. First, the icing wind tunnel ambient air was cooled down to freezing temperatures. Filtered air, which was then heated by an air heater installed in the line, was supplied to the spray nozzle to prevent the temperature from falling below freezing [54]. At an ambient air temperature of −20 °C, the tunnel fan was switched on and its speed was regulated to create an airflow of 40 m/s in the tunnel test section. Following this step, heated air and water were supplied to the spray nozzle at set pressures to produce a droplet cloud of 13 μm with an LWC of 2.8 g/m^3, and a pre-test spray commenced once the icing wind tunnel ambient air temperature reached −21 °C. The pre-test spray was a 45 s process, where a shield (shown in Figure 3a) was extended to prevent the pre-test spray droplets from impacting the test specimen. Right after the pre-test spray, the shield was retracted, and ice accretion began on

the test substrate for 120 s to produce an optimal ice height of 10–14 mm. It is crucial to obtain the optimal ice height before the initiation of the tensile test; Reference [59] proved that ice with a height of greater than 10 mm has little to no influence on ice adhesion measurement. Once the needed ice height was obtained, the shield was then extended back to its initial position, and the spray and the tunnel fan were turned off. The test sample (boss piece and substrate disc) was then left to cool down to −20 °C, as it typically experienced a temperature rise during the spray due to the latent heat rejection associated with the droplets' phase change being absorbed by the test sample. When the sample's temperature reached −20 °C, the tensile test was conducted; this consisted of turning the suction pump off and increasingly supplying air to the substrate disc via the 4 mm port hole at the rate of 131 kPa/sec until most or all of the ice detached from the surface. After the ice fracture occurred, the air pressure was lowered back to zero kPa. This test procedure was repeated 5 times for impact ice tests on both the aluminum and SLIC test substrates.

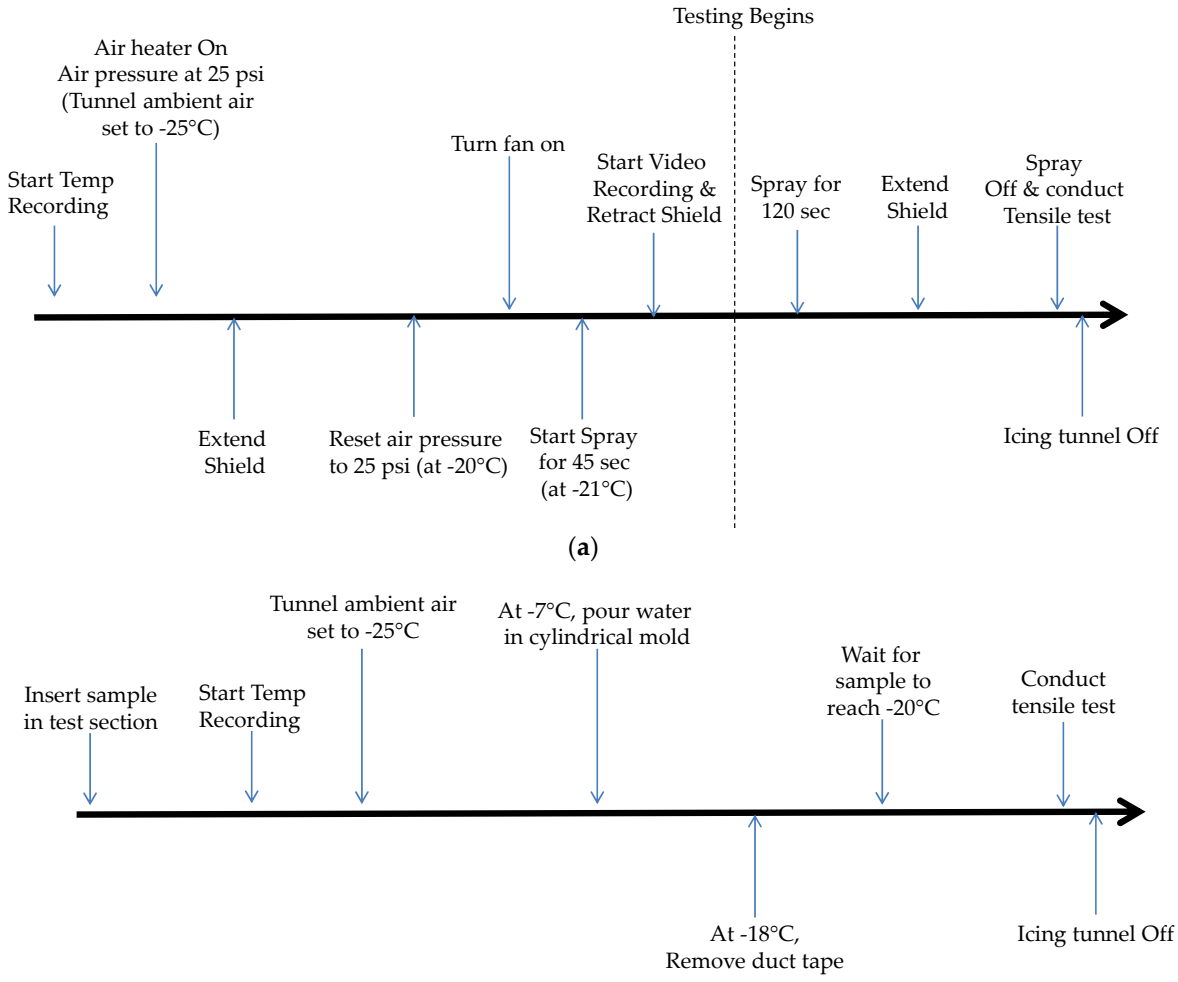

Figure 4. Sequences illustrating the test procedures for (**a**) impact ice and (**b**) static ice.

A time sequence depicting the static ice test steps is shown in Figure 4b. For static ice tests, a cylindrical mold was made to create a cylindrical ice block on the substrate discs to be tested. This mold was achieved by wrapping duct tape around the test sample. The purpose of the mold was to contain and hold water above the substrate disc surface while it slowly freezes. Once the cylindrical mold was formed around the test sample, it was then mounted onto the pressure pipe in the tunnel test section. At the tunnel ambient air temperature of −7 °C, deionized water (at room temperature of 22 °C) was slowly poured into the mold and left to slowly freeze as the tunnel ambient air continued to decrease

slowly. Following this step, the cylindrical mold was removed once the tunnel ambient air temperature reached −18 °C, a temperature where the water in the mold was assumed to be sufficiently frozen. The test sample temperature was then reduced to −20 °C, which after the tensile test was conducted following the same steps as for the impact test. Similarly, this test procedure was repeated 5 times for static ice tests on both the aluminum and SLIC test substrates.

3. Results and Discussion

3.1. Tensile Adhesion Test Results

As the gas pressure is applied and fracture occurs, the degree of ice detachment from the substrate can have three possible outcomes:

- A full cohesive fracture (leaving a complete layer of ice residue on the surface)
- A full adhesive fracture (leaving no ice residue on the surface)
- A mixed-mode fracture (leaving ice residue on only part of the surface)

For all of the tensile tests (both impact and static) conducted on the (non-coated) aluminum test substrate, a mixed-mode fracture was observed. For example, Figure 5 shows sample ice residues on the aluminum test substrate for both impact and static ice tests. However, the opposite happened in the case of the SLIC test substrate surface, where a full adhesive fracture occurred for all of the tests conducted, as shown by the sample test results in Figure 6. This outcome on the SLIC surface is a favorable demonstration of the properties of the SLIC coating, since a desired characteristic of an icephobic coating is its ability to facilitate the removal of ice. The average residual ice area for the present tests is given in Table 2, which quantifies the difference between adhesive and mixed-mode fractures.

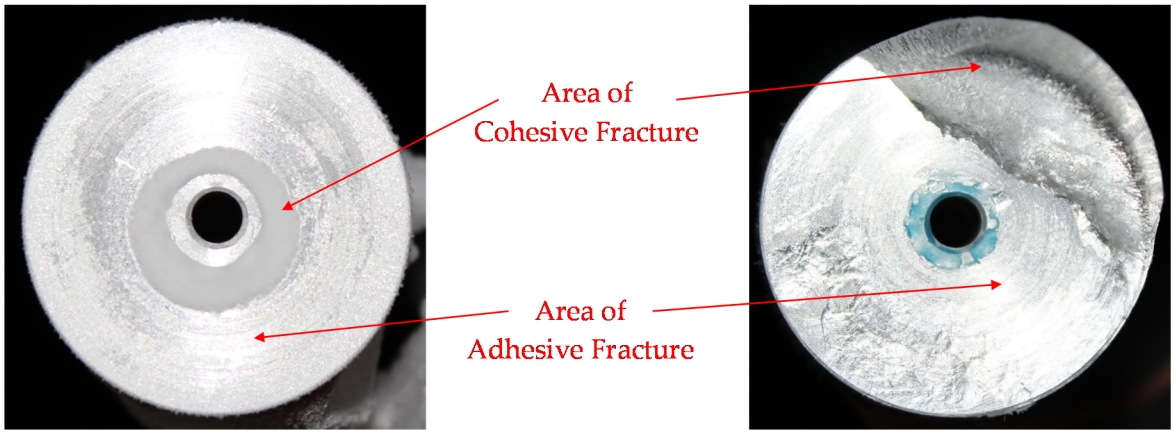

Figure 5. Residues left on the aluminum sample after ice tensile tests, shown by areas of adhesive and cohesive fractures for both conditions: (**a**) Impact ice and (**b**) static ice.

Table 2. Percentage of the cohesive ice residue area fraction recorded on aluminum and SLIC surfaces for both impact and static conditions.

Surfaces	Avg. % Cohesive Residue Area Fraction	
	Impact	Static
Al. Surface	20	44
SLIC Surface	0	0

(**a**) (**b**)

Figure 6. Full ice removal (100% adhesive failure) from the SLIC coating after ice tensile tests for: (**a**) Impact ice and (**b**) static ice.

In addition to the amount of ice remaining on the surface, there were also differences in how the ice was released once the fracture occurred. For the aluminum test substrate, the applied pressure launched the detached ice into the air as a projectile (see Video 2 in the Supplementary Materials). For the SLIC surface, the detached ice separated from the coating but remained suspended above the coating on an air cushion. In fact, the ice would then spin while suspended above the coating, indicating that the ice was indeed fully detached (see Video 4 in the Supplementary Materials). This levitation is due to the fact that the small amount of gas pressure being applied right after the ice detaches from the SLIC surface (still not enough to push the ice block off the surface) raises this one above the surface. Subsequently, as the gas pressure was increased, the detached ice eventually left the SLIC surface (see Video 4 in the Supplementary Materials).

The pressure at which the fracture occurred was also quite different for the different surfaces and conditions. For both the non-coated aluminum and the SLIC surfaces, the impact ice fracture pressure was consistently lower (and more repeatable) than that for the static ice tests. In addition, the critical air pressure for the SLIC surface was noted to be much lower (i.e., 50–80% less) than that for the aluminum surface. This observation confirmed the favorable attribute of the SLIC surface as having lower adhesion strength, which consequently could be used as an excellent de-icing tool in applications operating at extremely cold temperatures and where minimal force is needed for ice removal (e.g., gas turbine fan blades [3]). Using the critical pressure values, the residual ice area fraction (α, i.e., the fraction of the substrate disc area with residual ice after fracture), and the test geometry, ice tensile adhesion stress (σ_{te}) based on previously established methodology [29,31,54,55,59] was derived. At first, the fracture energy (FE) was computed using Equations (1)–(5), where 2γ and ω are the cohesive and adhesive ice fracture energies, respectively. In the equations, f_1 and f_2 are constants, ν is the Poisson's ratio for ice (taken as 0.35), c is the radius of the Teflon defect, H is the height of ice accretion, E is the Young's modulus of ice (taken as 8.5 GN·m^{-2}), and P_c is the critical air pressure required for ice fracture. Once the FE was obtained, the ice tensile stress (σ_{te}) was determined using Equations (6) and (7), where K_{Ic} is the fracture toughness.

$$FE = (2\gamma \times \alpha) + (1 - \alpha)\omega \quad (1)$$

$$2\gamma = \frac{P_c^2 \cdot c}{E \cdot f_1} \quad (2)$$

$$\omega = \frac{(P_c^2 \cdot c)}{E \cdot f_2} \quad (3)$$

$$f_1 = \frac{1}{1-\nu^2}\left\{\frac{3}{32}\left[\left(\frac{c}{H}\right)^3 + \left(\frac{c}{H}\right)\cdot\frac{4}{1-\nu}\right] + \frac{1}{\pi}\right\}^{-1} \quad (4)$$

$$f_2 = \frac{1}{1-\nu^2}\left\{\frac{3}{32}\left[\left(\frac{c}{H}\right)^3 + \left(\frac{c}{H}\right)\cdot\frac{4}{1-\nu}\right] + \frac{2}{\pi}\right\}^{-1} \quad (5)$$

$$\sigma_{te} = \frac{K_{Ic}}{\sqrt{\pi\cdot(2c)}} \quad (6)$$

$$K_{Ic} = \sqrt{\frac{FE\times E}{1-\nu^2}} \quad (7)$$

The individual tensile stress results for both the aluminum and SLIC surfaces are shown in Figure 7, where it can be seen that the adhesion was lower for impact tests compared to static tests, and much lower for SLIC compared to aluminum. This is consistent with the trends in fracture pressure.

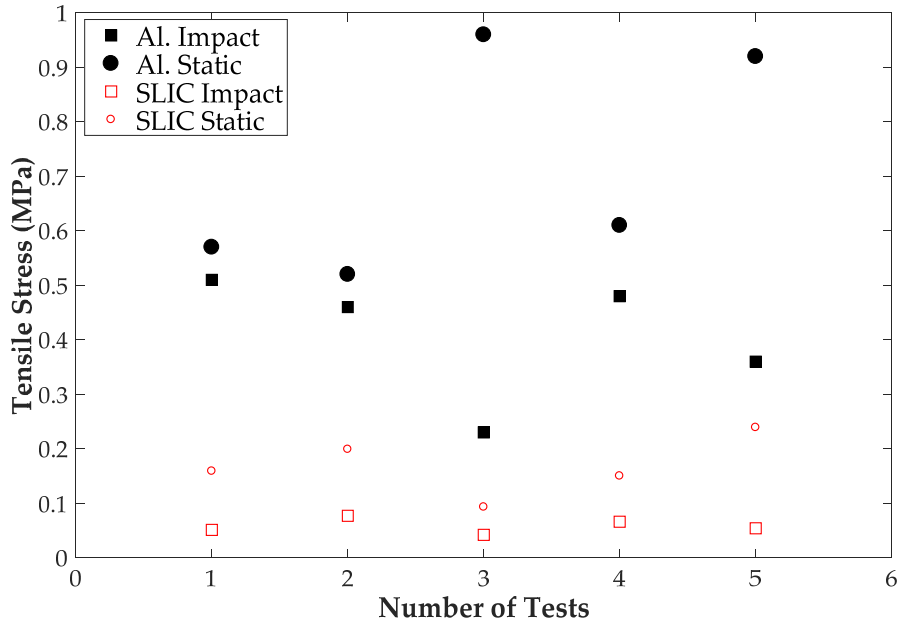

Figure 7. Ice adhesion tensile stress on aluminum and SLIC surfaces for impact and static ice conditions.

Based on the results in Figure 7, the ice tensile stress data were averaged. For the aluminum surface, the average ice tensile stress was found to be 0.41 MPa for the impact tests compared to 0.72 MPa for the static tests. For the SLIC surface, the average ice tensile stress was found to be 0.06 MPa for the impact tests compared to 0.17 MPa for the static tests. As a result, there was a reduction of 85% for SLIC as compared to aluminum for the impact tests and a reduction of 76% for the static tests. Overall, the SLIC surface displayed a reduction of more than half in terms of ice tensile adhesion stress compared to the aluminum surface, thus quantifying the favorable properties of the coating. This ice adhesion reduction in the case of the SLIC surface can be attributed to the low contact angle hysteresis or roll-off angle associated with the coating. In fact, several studies reported that icephobicity is highly dependent on roll-off angles [27,32,38,41,42,45,48,49,51,60]. Subsequently, the SLIC surface, with a much smaller roll-off angle (13° for SLIC compared to 27° for aluminum) displayed a low ice adhesion strength. Additionally, the lubricant layer at the coating surface coupled with the elastomer's high elasticity enable it with an interfacial slippage that enhances the release of the accreted ice release. This interfacial slippage is typical of icephobic-oil-infused elastomer coating [3,51]. Furthermore, it is to be noted that no significant degradation of this property was found, even after five tests on the same surface. This indicates surface resilience to icing conditions.

Another important aspect of the results in Figure 7 is that the adhesion strength was more consistent (displayed less scatter) for the SLIC surface as compared to the aluminum surface. This is attributed to the more stochastic nature of internal ice fracture associated with mixed-mode cohesive failure for detachment from aluminum surfaces [31,55,59,61]. A comparison of the present ice tensile adhesion data with that reported in the literature for hydrophobic/superhydrophobic coatings and metals in tensile mode is depicted in Figure 8. While the surface chemistry dominated the influence on ice adhesion, the variations are also associated with different icing conditions (temperature, air velocity, etc.), test procedures, and surface roughnesses (height and wavelength). However, the results show that static ice generally has a higher ice tensile adhesion strength compared to impact ice. Furthermore, the SLIC surface remains the best-performing surface (lowest tensile stress) among all of the results.

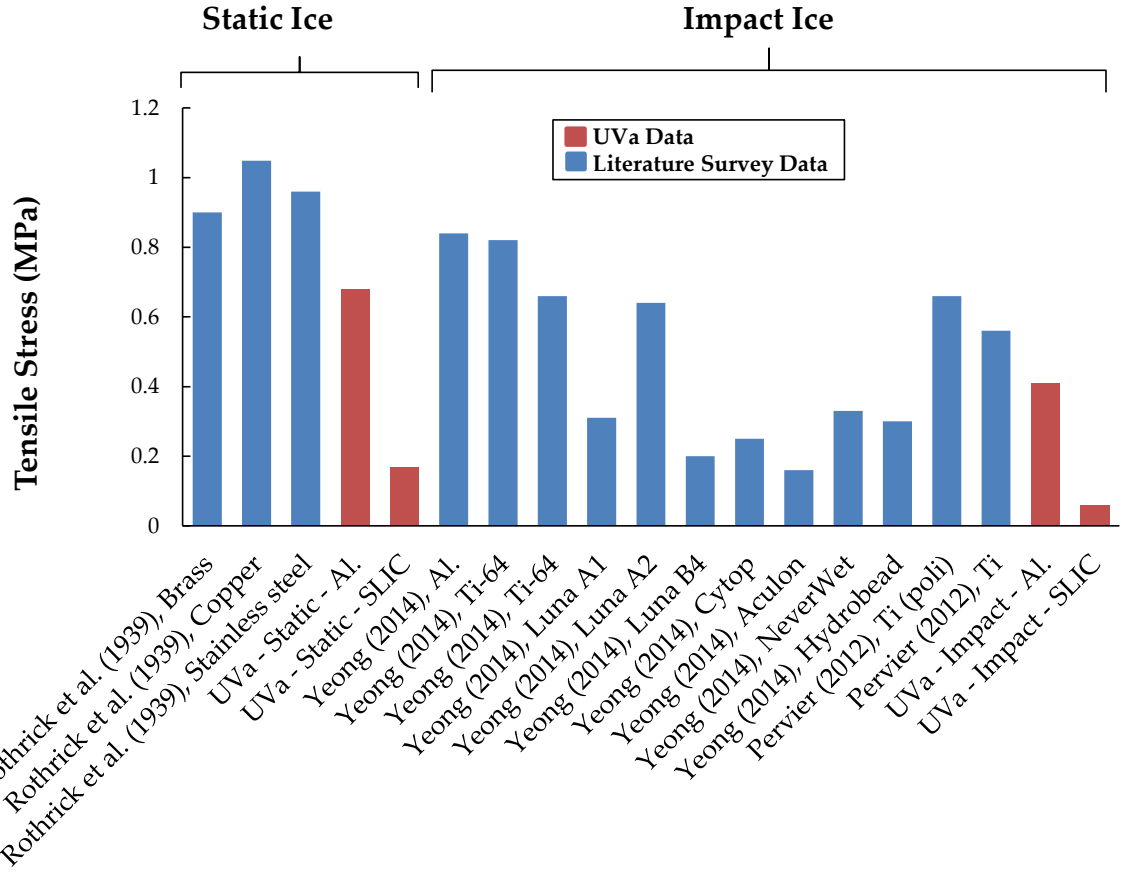

Figure 8. Tensile adhesion stress value comparison of this study (red bars) with previous data (blue bars) reported in the literature [55,59,62]. The results show that SLIC has far lower adhesion stress than any reported measurement on metal surfaces or hydrophobic/superhydrophobic coatings.

3.2. Durability of Wetting Properties

To further investigate the resilience of the SLIC coating to icing, wettability measurements were conducted on a regular flat aluminum surface coated with SLIC (used as a baseline) and on the two SLIC substrate discs used for the impact and static icing tests (where each was subjected to five icing tests). The results shown in Figure 9a,b and Table 3 revealed a slight enhancement of the coating's hydrophobic properties. In particular, the roll-off angles after the icing tests were actually somewhat lower, indicating that icing may help oil migrate to the surface to improve its icephobic performance. This evaluation confirms the durability of the SLIC's icephobicity with respect to icing in aerospace-based conditions.

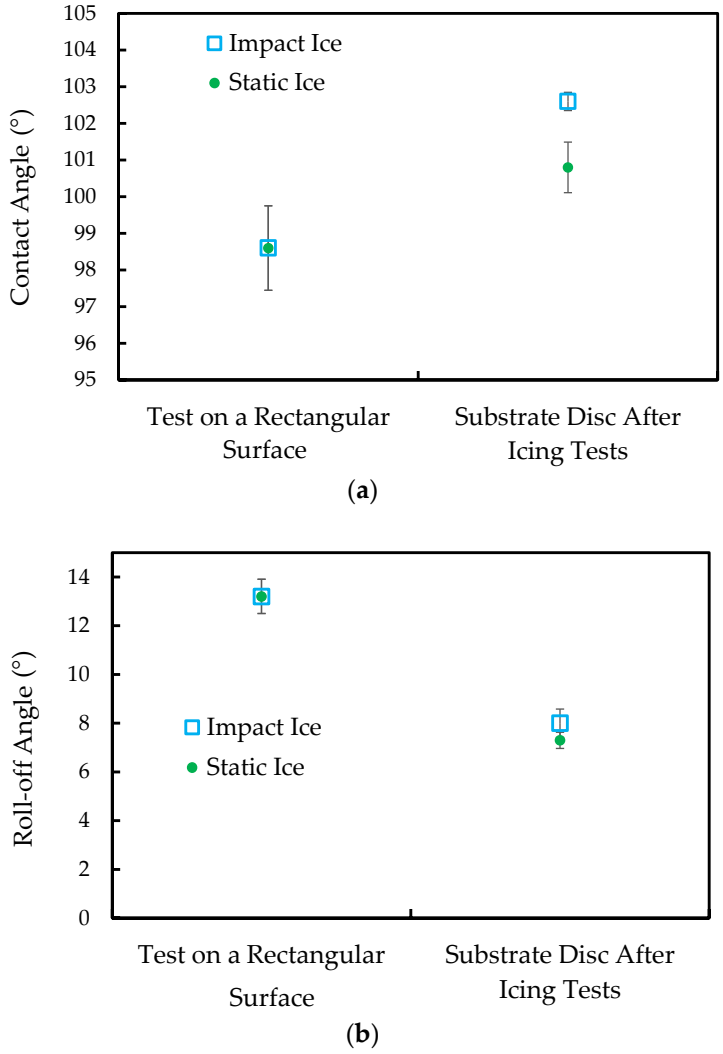

Figure 9. Measurements of the SLIC's wettability properties on a flat surface and on the tested SLIC test substrate after icing tests for both impact and static ice conditions, showing in (**a**) the contact angle and in (**b**) the roll-off angle.

Table 3. Measurement data plotted in Figure 9.

	Impact Ice		Static Ice	
	Contact Angle (°)	**Roll-off Angle (°)**	**Contact Angle (°)**	**Roll-off Angle (°)**
Test on a Rectangular Coupon	99	13	99	13
Substrate Disc After Icing Tests (SLIC)	102	8	101	7

3.3. Investigation of Mechanical Durability

While the SLIC maintained excellent durability for icing conditions, a more extreme test was to subject this coating to mechanical durability testing. This is important because a major concern of most icephobic coatings used to mitigate icing is their durability. In order to assess if this was an issue for the present hydrophobic SLIC surface, linear abrasion testing, a widely accepted method for qualitatively assessing non-wettable surfaces' mechanical durabilities, was conducted using a well-accepted abrasion technique [3,63]. This abrasion test consisted of a mechanical arm with an abrading tip which allows the installation of different types of abradants, as shown in Figure 10. The mechanical arm, along with its tip, could move in a linear motion upon contact with the surface

to be abraded and could be loaded with some weights to increase the force of abrasion. For this particular study, two types of abradants (medium-coarse abradant and crocking cloth) were used for the abrading tip, with a weight load of 373 g. Both mechanisms resulted in localized heating due to friction. In addition, the crocking cloth resulted in smoothing and some oil absorption of the SLIC coating, while the medium-coarse abradant resulted in micro-fracturing of the coating, since it contained abrasive particles similar to sandpaper particles.

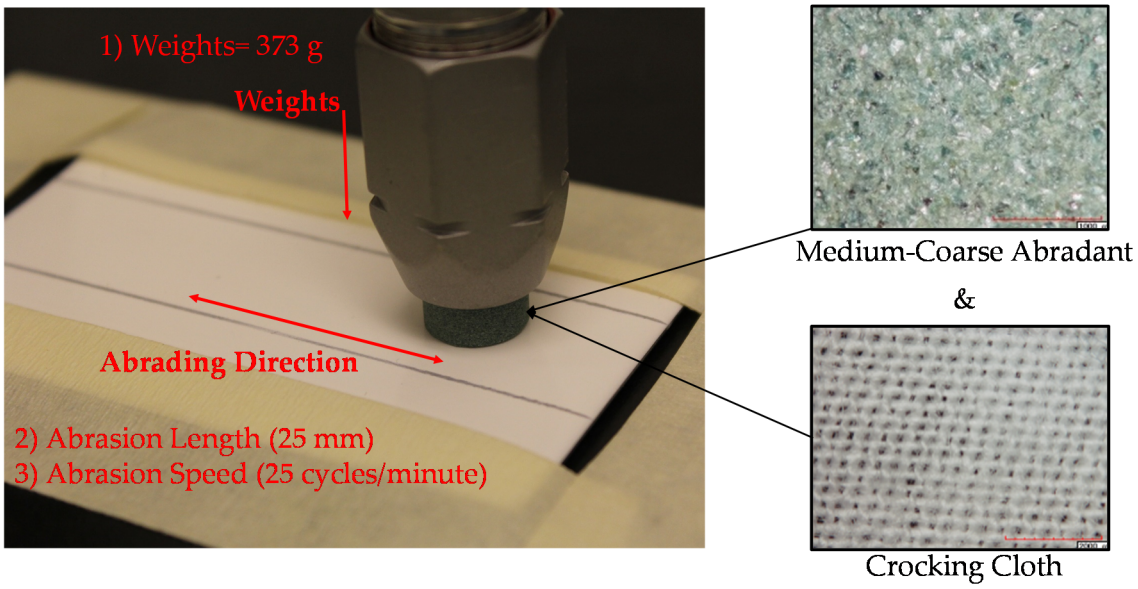

Figure 10. Durability testing on a rectangular surface with linear abrasion on a SLIC surface; the right-hand-side images show two types of abradants: A medium-coarse abradant and a crocking cloth [3].

Once the SLIC coating was secured underneath the abrading tip, the mechanical arm was actuated to operate 20 cycles, where one cycle corresponds to the abrading tip going the 25 mm abrasion length on the coating in one direction and back. A video of this mechanical abrasion test, as well as the post-abrasion images of the SLIC, are provided in the Supplementary Materials. After all of the linear abrasion cycles were completed for either the crocking cloth or the medium-coarse abradant, wettability was measured in terms of static contact angle and roll-off angle. As seen in Figure 11 and Table 4, the roll-off angle substantially increased (the performance degraded) for both abradant types, whereas the contact angle did not vary as much (the SLIC surfaces remained hydrophobic). However, four days after the abrasion test, the measurement of the wettability properties was repeated on the same samples (one each, abraded by the crocking cloth and the medium-coarse abradant). This time, the measurement revealed that the roll-off angles for both samples recovered to their original (before abrasion) value, while the hydrophobic contact angle was preserved. This demonstrates the self-healing ability of the coating; hence, the term "self-lubricating" used for the name of the coating. This self-healing ability is attributed to the high flexibility of the polymeric chain of the elastomer, enabling the oil particles in the matrix to migrate within this one and towards the surface. This behavior of polymers (or polymer-based coating) of allowing the migration of an introduced self-healing agent (oil in this study) is very typical, and is also described in other researches [50,64,65]. Notably, in Reference [50], the self-healing agent enables the coating to recover its texture, while the oil in the SLIC (self-healing agent in the coating described in this study) helps recover the coating wettability properties and functionality. Overall, this assessment shows the ability of the coating to withstand light and gradual damage that may be caused to the coating in a realistic environment. As a future study, it is recommended that ice adhesion after abrasion be measured to further investigate the durability of the SLIC.

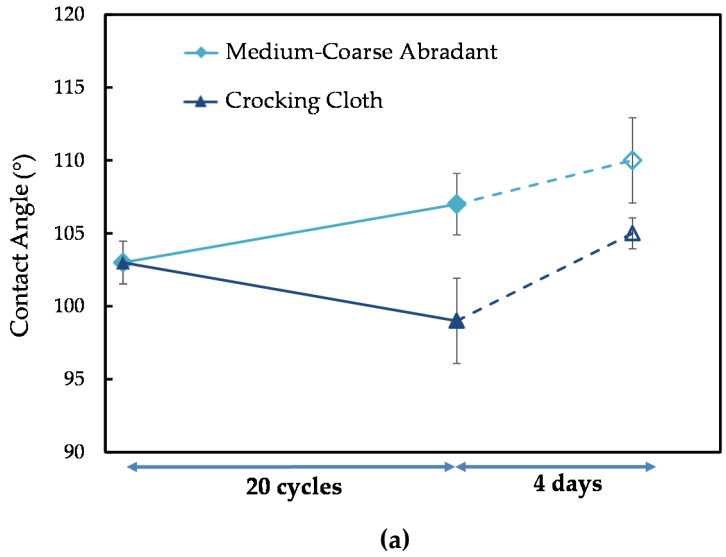

Figure 11. Present measurements of SLIC wettability before and after abrasion with a medium-coarse abradant and a crocking cloth, showing in (**a**) the contact angle and in (**b**) the roll-off angle.

Table 4. Measurement data plotted in Figure 11.

Abradants	Contact Angle (°)			Roll-off Angle (°)		
	Zero Cycle	After 20 Cycles	After 4 Days	Zero Cycle	After 20 Cycles	After 4 Days
Medium-Coarse Abradant	103	107	110	17	46	21
Crocking Cloth	103	99	105	17	46	16

4. Conclusions

In this study, an icing wind tunnel was used to measure ice adhesion tensile strength on a self-lubricating icephobic coating (SLIC) surface and aluminum surface for both impact and static ice conditions. The static ice consisted of deionized water contained in a cylindrical mold left to freeze over time on the tested surfaces at a temperature of −20 °C. On the other hand, the impact ice was ice formed from 13 μm droplets hitting the tested surfaces at a velocity of 40 m/s and at a temperature of −20 °C,

freezing during the process. The results showed that generally, impact ice has a tensile adhesion strength lower than that of static ice. Additionally, the SLIC surface reduced the ice tensile adhesion strength by more than 50% for both impact and static ice conditions. Subsequently, this functionality makes the SLIC surface a good candidate as a de-icing tool for applications where minimal force would be required for ice removal. Additionally, the SLIC surface showed good resilience during the icing tests. In particular, even after five icing tests, the tensile stress did not significantly increase (ice adhesion did not degrade) and the roll-off angle did not significantly increase (wettability did not degrade). This resilience of the coating's hydrophobicity (contact angle and roll-off angle) was demonstrated for both impact and static icing tests. To examine the coating's robustness to mechanical abrasion, tests were conducted with a linear abrader. After the application of 20 cycles, the tests revealed some degradation of the contact and roll-off angles taken for the SLIC coating. However, a full recovery of these properties was noted when measurements were taken four days after the abrasion testing. This indicates a self-healing ability associated with the SLIC for these conditions.

Supplementary Materials: The following are available online at http://www.mdpi.com/2079-6412/10/3/262/s1, Video S1: GoPro recording (sped up to X8) of the impact ice accretion on the aluminum surface in the icing wind tunnel test section, Video S2: GoPro recording (sped up to X8) of the tensile test or pop-off test on the aluminum surface, Video S3: GoPro recording (sped up to X4) of the impact ice accretion on the SLIC surface in the icing wind tunnel test section, Video S4: GoPro recording (sped up to X2) of the tensile test or pop-off test on the SLIC surface, Video S5. Video showing the linear abrasion test on the SLIC using the medium-coarse abradant, Figure S1: CANON photographic camera and HIROX microscope images of the SLIC coating post-abrasion.

Author Contributions: All authors have read and agreed to the published version of the manuscript and equally shared in all aspects. Conceptualization, E.T. and E.L.; methodology, E.T. and E.L.; validation, E.T. and E.L.; formal analysis, E.T. and E.L.; investigation, E.T. and E.L.; resources, E.T. and E.L.; data curation, E.T. and E.L.; writing—original draft preparation, E.T. and E.L.; writing—review and editing, E.T. and E.L.; visualization, E.T. and E.L.; funding acquisition, E.T. and E.L.

Funding: This research received no external funding.

Acknowledgments: The authors would like to acknowledge Michael Jeong, who was instrumental in obtaining and processing data.

Conflicts of Interest: The authors declare no conflict of interest.

References

1. Gent, R.W.; Dart, N.P.; Cansdale, J.T. Aircraft icing. *Philos. Trans. R. Soc. London Ser. A Math. Phys. Eng. Sci.* **2000**, *358*, 2873–2911. [CrossRef]
2. Jin, Z.; Hu, H. Icing process of small water droplets impinging onto a frozen cold plate. *J. Thermophys. Heat Transf.* **2010**, *24*, 841–844. [CrossRef]
3. Yeong, Y.H.; Milionis, A.; Loth, E.; Sokhey, J. Self-lubricating icephobic elastomer coating (SLIC) for ultralow ice adhesion with enhanced durability. *Cold Reg. Sci. Technol.* **2018**, *148*, 29–37. [CrossRef]
4. Yirtici, O.; Tuncer, I.H.; Ozgen, S. Ice accretion prediction on wind turbines and consequent power losses. *J. Phys. Conf. Ser.* **2016**, *753*, 022022. [CrossRef]
5. Jasinski, W.J.; Noe, S.C.; Selig, M.S.; Bragg, M.B. Wind turbine performance under icing conditions. *J. Sol. Energy Eng.* **1998**, *120*, 60–65. [CrossRef]
6. Dalili, N.; Edrisy, A.; Carriveau, R. A review of surface engineering issues critical to wind turbine performance. *Renew. Sustain. Energy Rev.* **2009**, *13*, 428–438. [CrossRef]
7. Antonini, C.; Innocenti, M.; Horn, T.; Marengo, M.; Amirfazli, A. Understanding the effect of superhydrophobic coatings on energy reduction in anti-icing systems. *Cold Reg. Sci. Technol.* **2011**, *67*, 58–67. [CrossRef]
8. Boinovich, L.B.; Emelyanenko, A.M. Anti-icing potential of superhydrophobic coatings. *Mendeleev Commun.* **2013**, *23*, 3–10. [CrossRef]
9. Schutzius, T.M.; Jung, S.; Maitra, T.; Eberle, P.; Antonini, C.; Stamatopoulos, C.; Poulikakos, D. Physics of icing and rational design of surfaces with extraordinary icephobicity. *Langmuir* **2015**, *31*, 4807–4821. [CrossRef]

10. Zheng, S.; Li, C.; Fu, Q.; Hu, W.; Xiang, T.; Wang, Q.; Du, M.; Liu, X.; Chen, Z. Development of stable superhydrophobic coatings on aluminum surface for corrosion-resistant, self-cleaning, and anti-icing applications. *Mater. Des.* **2016**, *93*, 261–270. [CrossRef]
11. Susoff, M.; Siegmann, K.; Pfaffenroth, C.; Hirayama, M. Evaluation of icephobic coatings—Screening of different coatings and influence of roughness. *Appl. Surf. Sci.* **2013**, *282*, 870–879. [CrossRef]
12. Cao, L.; Jones, A.K.; Sikka, V.K.; Wu, J.; Gao, D. Anti-Icing superhydrophobic coatings. *Langmuir* **2009**, *25*, 12444–12448. [CrossRef]
13. Chavan, S.; Carpenter, J.; Nallapaneni, M.; Chen, J.Y.; Miljkovic, N. Bulk water freezing dynamics on superhydrophobic surfaces. *Appl. Phys. Lett.* **2017**, *110*, 041604. [CrossRef]
14. Chavan, S.; Park, D.; Singla, N.; Sokalski, P.; Boyina, K.; Miljkovic, N. Effect of latent heat released by freezing droplets during frost wave propagation. *Langmuir* **2018**, *34*, 6636–6644. [CrossRef] [PubMed]
15. De Koninck, L.H.; Ahmadi, S.F.; Boreyko, J.B. Passive anti-frosting cables. *Int. J. Heat Mass Transf.* **2020**, *146*, 118808. [CrossRef]
16. Esmeryan, K.D.; Bressler, A.H.; Castano, C.E.; Fergusson, C.P.; Mohammadi, R. Rational strategy for the atmospheric icing prevention based on chemically functionalized carbon soot coatings. *Appl. Surf. Sci.* **2016**, *390*, 452–460. [CrossRef]
17. Esmeryan, K.D.; Castano, C.E.; Mohammadi, R.; Lazarov, Y.; Radeva, E.I. Delayed condensation and frost formation on superhydrophobic carbon soot coatings by controlling the presence of hydrophilic active sites. *J. Phys. D Appl. Phys.* **2018**, *51*, 055302. [CrossRef]
18. Farhadi, S.; Farzaneh, M.; Kulinich, S.A. Anti-icing performance of superhydrophobic surfaces. *Appl. Surf. Sci.* **2011**, *257*, 6264–6269. [CrossRef]
19. Liu, Y.; Li, L.; Li, H.; Hu, H. An experimental study of surface wettability effects on dynamic ice accretion process over an UAS propeller model. *Aerosp. Sci. Technol.* **2018**, *73*, 164–172. [CrossRef]
20. Wang, N.; Xiong, D.; Deng, Y.; Shi, Y.; Wang, K. Mechanically robust superhydrophobic steel surface with anti-icing, UV-durability, and corrosion resistance properties. *ACS Appl. Mater. Interfaces* **2015**, *7*, 6260–6272. [CrossRef]
21. Verho, T.; Bower, C.; Andrew, P.; Franssila, S.; Ikkala, O.; Ras, R.H.A. Mechanically durable superhydrophobic surfaces. *Adv. Mater.* **2011**, *23*, 673–678. [CrossRef]
22. Ellinas, K.; Tserepi, A.; Gogolides, E. Durable superhydrophobic and superamphiphobic polymeric surfaces and their applications: A review. *Adv. Colloid Interface Sci.* **2017**, *250*, 132–157. [CrossRef]
23. Balordi, M.; Cammi, A.; Santucci de Magistris, G.; Chemelli, C. Role of micrometric roughness on anti-ice properties and durability of hierarchical super-hydrophobic aluminum surfaces. *Surf. Coat. Technol.* **2019**, *374*, 549–556. [CrossRef]
24. Boinovich, L.B.; Emelyanenko, A.M.; Ivanov, V.K.; Pashinin, A.S. Durable icephobic coating for stainless steel. *ACS Appl. Mater. Interfaces* **2013**, *5*, 2549–2554. [CrossRef]
25. Song, J.; Zhao, D.; Han, Z.; Xu, W.; Lu, Y.; Liu, X.; Liu, B.; Carmalt, C.J.; Deng, X.; Parkin, I.P. Super-robust superhydrophobic concrete. *J. Mater. Chem. A* **2017**, *5*, 14542–14550. [CrossRef]
26. Kulinich, S.A.; Farhadi, S.; Nose, K.; Du, X.W. Superhydrophobic surfaces: Are they really ice-repellent? *Langmuir* **2011**, *27*, 25–29. [CrossRef]
27. Kim, P.; Wong, T.S.; Alvarenga, J.; Kreder, M.J.; Adorno-Martinez, W.E.; Aizenberg, J. Liquid-infused nanostructured surfaces with extreme anti-ice and anti-frost performance. *ACS Nano* **2012**, *6*, 6569–6577. [CrossRef]
28. Esmeryan, K.D. From extremely water-repellent coatings to passive icing protection—principles, limitations and innovative application aspects. *Coatings* **2020**, *10*, 66. [CrossRef]
29. Yeong, Y.H.; Loth, E.; Sokhey, J. Ice adhesion on superhydrophobic coatings in a icing wind tunnel. In *Advances in Polymer Science*; Springer: Berlin/Heidelberg, Germany, 2017.
30. Maitra, T.; Jung, S.; Giger, M.E.; Kandrical, V.; Ruesch, T.; Poulikakos, D. Superhydrophobicity vs. ice adhesion: The quandary of robust icephobic surface design. *Adv. Mater. Interfaces* **2015**, *2*, 1500330. [CrossRef]
31. Yeong, Y.H.; Milionis, A.; Loth, E.; Sokhey, J.; Lambourne, A. Atmospheric ice adhesion on water-repellent coatings: Wetting and surface topology effects. *Langmuir* **2015**, *31*, 13107–13116. [CrossRef]
32. Kreder, M.J.; Alvarenga, J.; Kim, P.; Aizenberg, J. Design of anti-icing surfaces: Smooth, textured or slippery? *Nat. Rev. Mater.* **2016**, *1*, 1–15. [CrossRef]

33. Jung, S.; Dorrestijn, M.; Raps, D.; Das, A.; Megaridis, C.M.; Poulikakos, D. Are superhydrophobic surfaces best for icephobicity? *Langmuir* **2011**, *27*, 3059–3066. [CrossRef] [PubMed]
34. Wier, K.A.; McCarthy, T.J. Condensation on ultrahydrophobic surfaces and its effect on droplet mobility: Ultrahydrophobic surfaces are not always water repellant. *Langmuir* **2006**, *22*, 2433–2436. [CrossRef]
35. Wilson, P.W.; Lu, W.; Xu, H.; Kim, P.; Kreder, M.J.; Alvarenga, J.; Aizenberg, J. Inhibition of ice nucleation by slippery liquid-infused porous surfaces (SLIPS). *Phys. Chem. Chem. Phys.* **2013**, *15*, 581–585. [CrossRef]
36. Smith, J.D.; Dhiman, R.; Anand, S.; Reza-Garduno, E.; Cohen, R.E.; McKinley, G.H.; Varanasi, K.K. Droplet mobility on lubricant-impregnated surfaces. *Soft Matter* **2013**, *9*, 1772–1780. [CrossRef]
37. Subramanyam, S.B.; Rykaczewski, K.; Varanasi, K.K. Ice adhesion on lubricant-impregnated textured surfaces. *Langmuir* **2013**, *29*, 13414–13418. [CrossRef]
38. Ozbay, S.; Yuceel, C.; Erbil, H.Y. Improved icephobic properties on surfaces with a hydrophilic lubricating liquid. *ACS Appl. Mater. Interfaces* **2015**, *7*, 22067–22077. [CrossRef]
39. Rykaczewski, K.; Anand, S.; Subramanyam, S.B.; Varanasi, K.K. Mechanism of frost formation on lubricant-impregnated surfaces. *Langmuir* **2013**, *29*, 5230–5238. [CrossRef]
40. Wong, T.S.; Kang, S.H.; Tang, S.K.Y.; Smythe, E.J.; Hatton, B.D.; Grinthal, A.; Aizenberg, J. Bioinspired self-repairing slippery surfaces with pressure-stable omniphobicity. *Nature* **2011**, *477*, 443–447. [CrossRef]
41. Wang, G.; Guo, Z. Liquid infused surfaces with anti-icing properties. *Nanoscale* **2019**, *11*, 22615–22635. [CrossRef]
42. Erbil, H.Y. Improvement of lubricant-infused surfaces for anti-icing applications. *Surf. Innov.* **2016**, *4*, 214–217. [CrossRef]
43. Zhang, M.; Yu, J.; Chen, R.; Liu, Q.; Liu, J.; Song, D.; Liu, P.; Gao, L.; Wang, J. Highly transparent and robust slippery lubricant-infused porous surfaces with anti-icing and anti-fouling performances. *J. Alloy. Compd.* **2019**, *803*, 51–60. [CrossRef]
44. Zhu, L.; Xue, J.; Wang, Y.; Chen, Q.; Ding, J.; Wang, Q. Ice-phobic coatings based on silicon-oil-infused polydimethylsiloxane. *ACS Appl. Mater. Interfaces* **2013**, *5*, 4053–4062. [CrossRef]
45. Wang, Y.; Yao, X.; Chen, J.; He, Z.; Liu, J.; Li, Q.; Wang, J.; Jiang, L. Organogel as durable anti-icing coatings. *Sci. China Mater.* **2015**, *58*, 559–565. [CrossRef]
46. Urata, C.; Dunderdale, G.J.; England, M.W.; Hozumi, A. Self-lubricating organogels (SLUGs) with exceptional syneresis-induced anti-sticking properties against viscous emulsions and ices. *J. Mater. Chem. A* **2015**, *3*, 12626–12630. [CrossRef]
47. Liu, H.; Zhang, P.; Liu, M.; Wang, S.; Jiang, L. Organogel-based thin films for self-cleaning on various surfaces. *Adv. Mater.* **2013**, *25*, 4477–4481. [CrossRef]
48. Eifert, A.; Paulssen, D.; Varanakkottu, S.N.; Baier, T.; Hardt, S. Simple fabrication of robust water-repellent surfaces with low contact-angle hysteresis based on impregnation. *Adv. Mater. Interfaces* **2014**, *1*, 1300138. [CrossRef]
49. Damle, V.G.; Uppal, A.; Sun, X.; Burgin, T.P.; Rykaczewski, K. Rapid and scalable lubrication and replenishment of liquidinfused materials. *Surf. Innov.* **2015**, *4*, 102–108. [CrossRef]
50. Zhuo, Y.; Håkonsen, V.; He, Z.; Xiao, S.; He, J.; Zhang, Z. Enhancing the mechanical durability of icephobic surfaces by introducing autonomous self-healing function. *ACS Appl. Mater. Interfaces* **2018**, *10*, 11972–11978. [CrossRef]
51. Golovin, K.; Kobaku, S.P.R.; Lee, D.H.; DiLoreto, E.T.; Mabry, J.M.; Tuteja, A. Designing durable icephobic surfaces. *Sci. Adv.* **2016**, *2*, 1501496. [CrossRef]
52. Potapczuk, M.G. Aircraft icing research at NASA glenn research center. *J. Aerosp. Eng.* **2013**, *26*, 260–276. [CrossRef]
53. Acker, L.W. *Preliminary Results of Natural Icing of an Axial-Flow Turbojet Engine*; NACA Research Memorandum: Washington, DC, USA, 1948.
54. Tetteh, E.Y.; Loth, E.; Loebig, J.; Cummings, J.; Lilly, N. The compact icing research tunnel (CIRT). In Proceedings of the AIAA Propulsion and Energy 2019 Forum, Indianapolis, IN, USA, 19–22 August 2019.
55. Yeong, Y.H. Impinging Drops on Superhydrophobic Surfaces at Icing Conditions. Ph.D. Thesis, University of Virginia, Charlottesville, VA, USA, April 2014.
56. Andrews, E.H.; Lockington, N.A. The cohesive and adhesive strength of ice. *J. Mater. Sci.* **1983**, *18*, 1455–1465. [CrossRef]

57. Andrews, E.H.; Majid, H.A.; Lockington, N.A. Adhesion of ice to a flexible substrate. *J. Mater. Sci.* **1984**, *19*, 73–81. [CrossRef]
58. Andrews, E.H.; Stevenson, A. Fracture energy of epoxy resin under plane strain conditions. *J. Mater. Sci.* **1978**, *13*, 1680–1688. [CrossRef]
59. Pervier, M.-L. Mechanics of Ice Detachment Applied To Turbomachinery. Ph.D. Thesis, Cranfield University, Bedford, UK, 2012.
60. Meuler, A.J.; Smith, J.D.; Varanasi, K.K.; Mabry, J.M.; McKinley, G.H.; Cohen, R.E. Relationships between water wettability and ice adhesion. *ACS Appl. Mater. Interfaces* **2010**, *2*, 3100–3110. [CrossRef]
61. Chu, M.; Scavuzzo, R.; Kellackey, C. Tensile properties of impact ices. In Proceedings of the 30th Aerospace Sciences Meeting and Exhibit, Reno, NV, USA, 6–9 January 1992.
62. Rothrock, A.M.; Selden, R.F. *Adhesion of Ice in its Relation to the De-Icing of Airplanes*; National Advisory Committee for Aeronautics: Washington, DC, USA, 1939.
63. Milionis, A.; Loth, E.; Bayer, I.S. Recent advances in the mechanical durability of superhydrophobic materials. *Adv. Colloid Interface Sci.* **2016**, *229*, 57–79. [CrossRef]
64. Cho, S.H.; White, S.R.; Braun, P.V. Self-healing polymer coatings. *Adv. Mater.* **2009**, *21*, 645–649. [CrossRef]
65. Zhuo, Y.; Xiao, S.; Håkonsen, V.; Li, T.; Wang, F.; He, J.; Zhang, Z. Ultrafast self-healing and highly transparent coating with mechanically durable icephobicity. *Appl. Mater. Today* **2020**, *19*, 100542. [CrossRef]